**Table S1** Main parameters prescribed for each biome type in the carbon model, including maximum light use efficiency (ε_{max}), carbon use efficiency (CUE), the extinction coefficient of root distribution (β), fraction (percentage) of leaf, fine root and woody components of litterfall.

| Biome type	ε_{max} (g C MJ^{-1})	CUE	β^*	Leaf (%)	Fine roots (%)	Wood (%)
Grasslands/Herbaceous	0.50	0.60	0.914	32	48	20
Scrub/Shrub	0.78	0.575	0.930	28	42	30
Forest	1.05	0.55	0.943	24	36	40
Wetland	1.00	0.60	0.914	36	54	10
Croplands	1.20	0.60	0.914	28	42	30

* The vertical root distribution was defined as in Jackson et al. (1996): $\gamma = 1 - \beta^z$, where γ is the cumulative root fraction from soil surface to depth z (cm), and β is the extinction coefficient parameter.
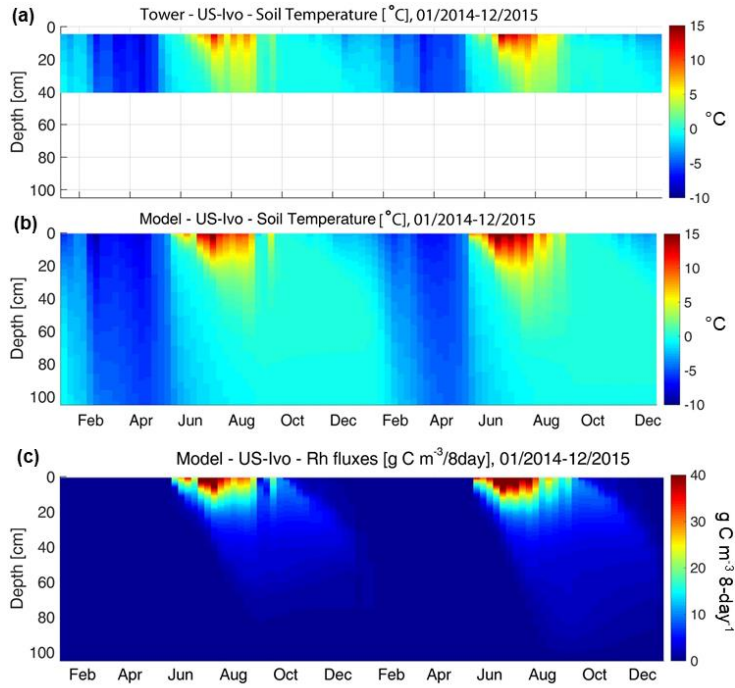
Fig. S1 Model simulated soil temperature and heterotrophic respiration (Rh) flux density profile comparing with in-situ soil temperature profile (up to 40 cm) at the US-Ivo site from 2014 to 2015.
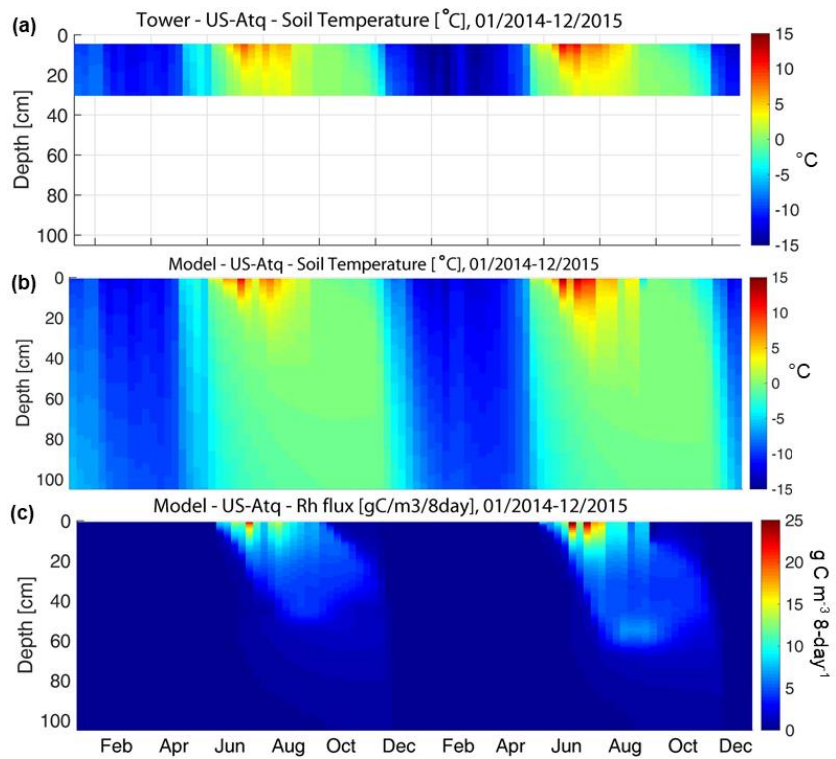
Fig. S2 Model simulated soil temperature and heterotrophic respiration (Rh) flux density profile, comparing with in-situ soil temperature profile (up to 30 cm) at the US-Atq site from 2014 to 2015.
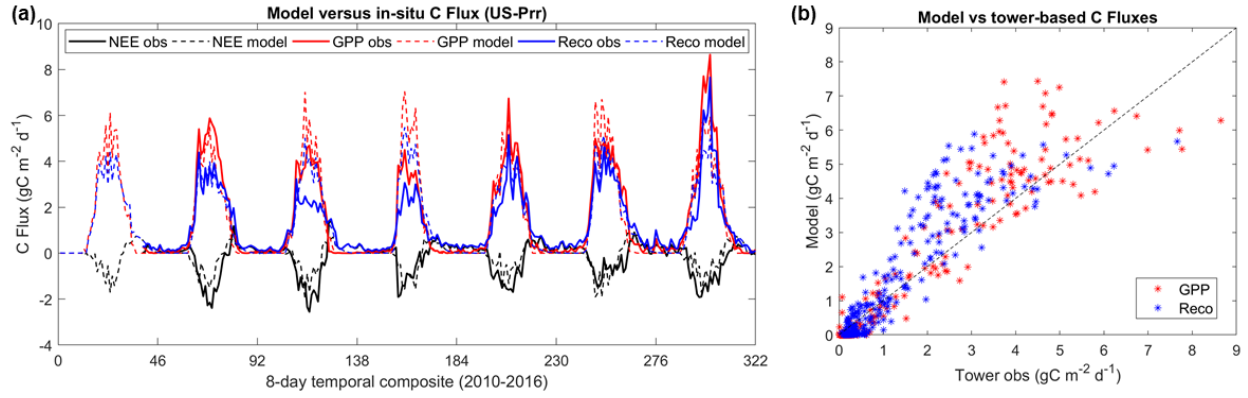
Fig. S3 Comparison of model simulated carbon fluxes with EC tower-based NEE measurements and GPP/Reco estimates at US-Prr site.
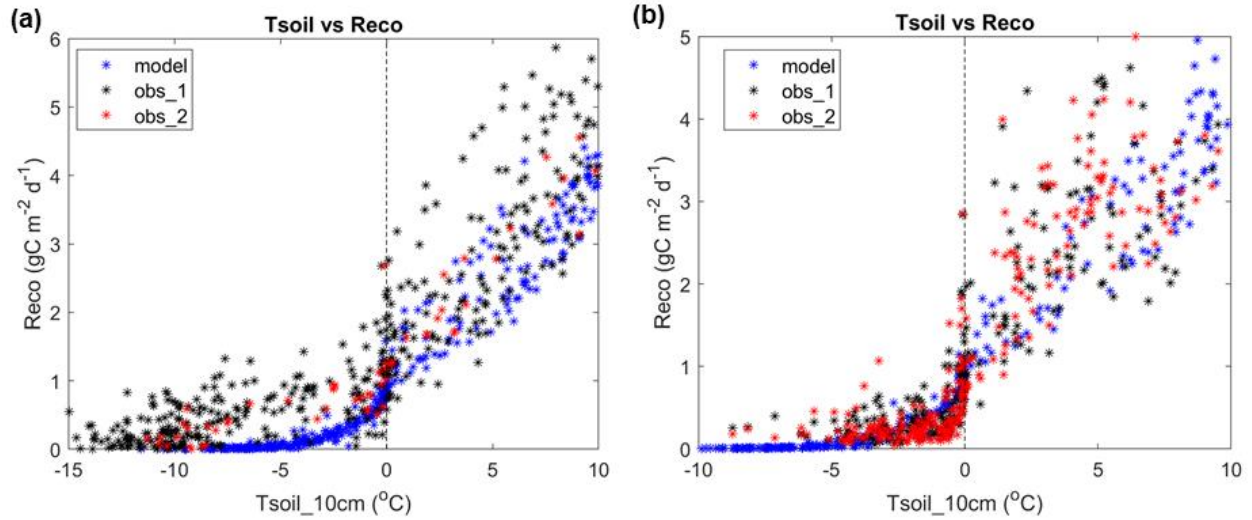
Fig. S4 Relationship between soil temperature (Tsoil) at ~10 cm depth and Reco at the two boreal forest sites: (a) US-Uaf: obs_1 and obs_2 use Tsoil measurements at different soil nodes. At this site, only one set of GPP and Reco estimates was provided by the tower PI. (b) US-Prr: obs_1 and obs_2 use tower-based Reco estimates derived from NEE observations and different partitioning methods provided by the tower PI.
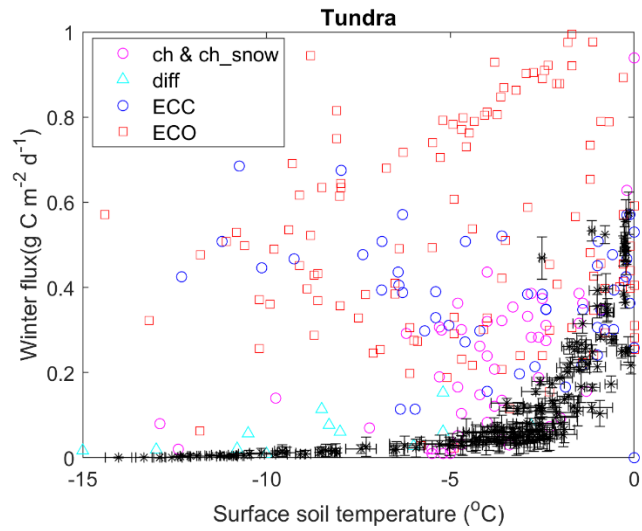
Fig. S5 Effects of soil temperature on winter CO_2 fluxes at all Alaskan tundra sites using the in-situ synthesis data collected from different methods (Natali et al. 2019b). EC-open path (ECO) measurements show a large scattering in the temperature response of winter flux than the other methods. Model simulated temperature response of winter soil respiration was indicated by Asterisk.
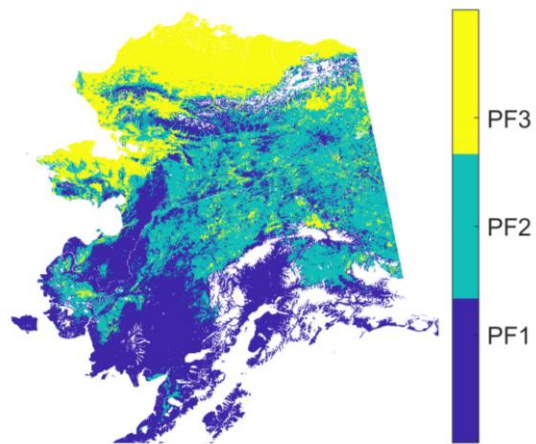
Fig. S6 The permafrost zonal map in Alaska, based on an ancillary permafrost map (Pastick et al., 2015), including permafrost frequency ranging from 0 to 33.3% (PF1), from 33.3% to 66.7% (PF2), from 66.7% to 100% (PF3).
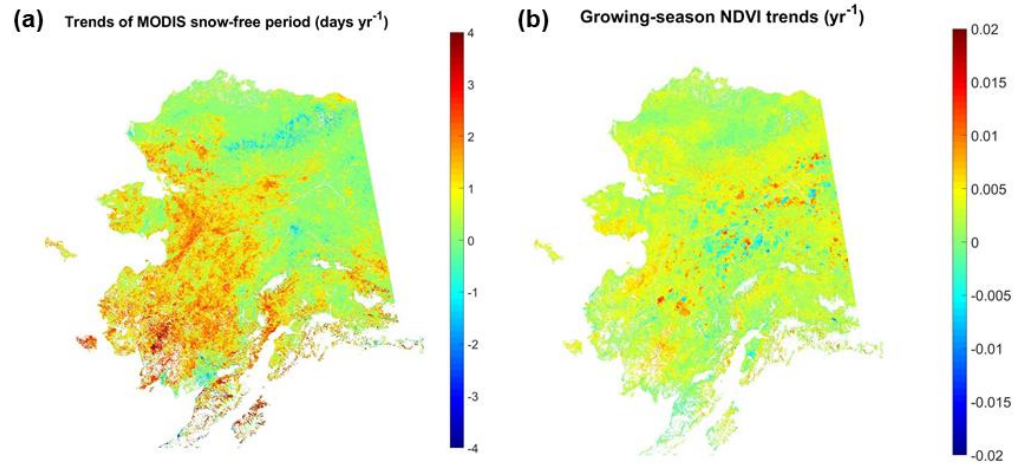
Fig. S7 Annual GPP trends (Fig. 7a) are mostly explained by a longer growing season (or snow-free season, a) and positive NDVI trends (b) during the growing season (May-September) from 2001 to 2017. The snow-free period in panel (a) was derived from MODIS SCE data.
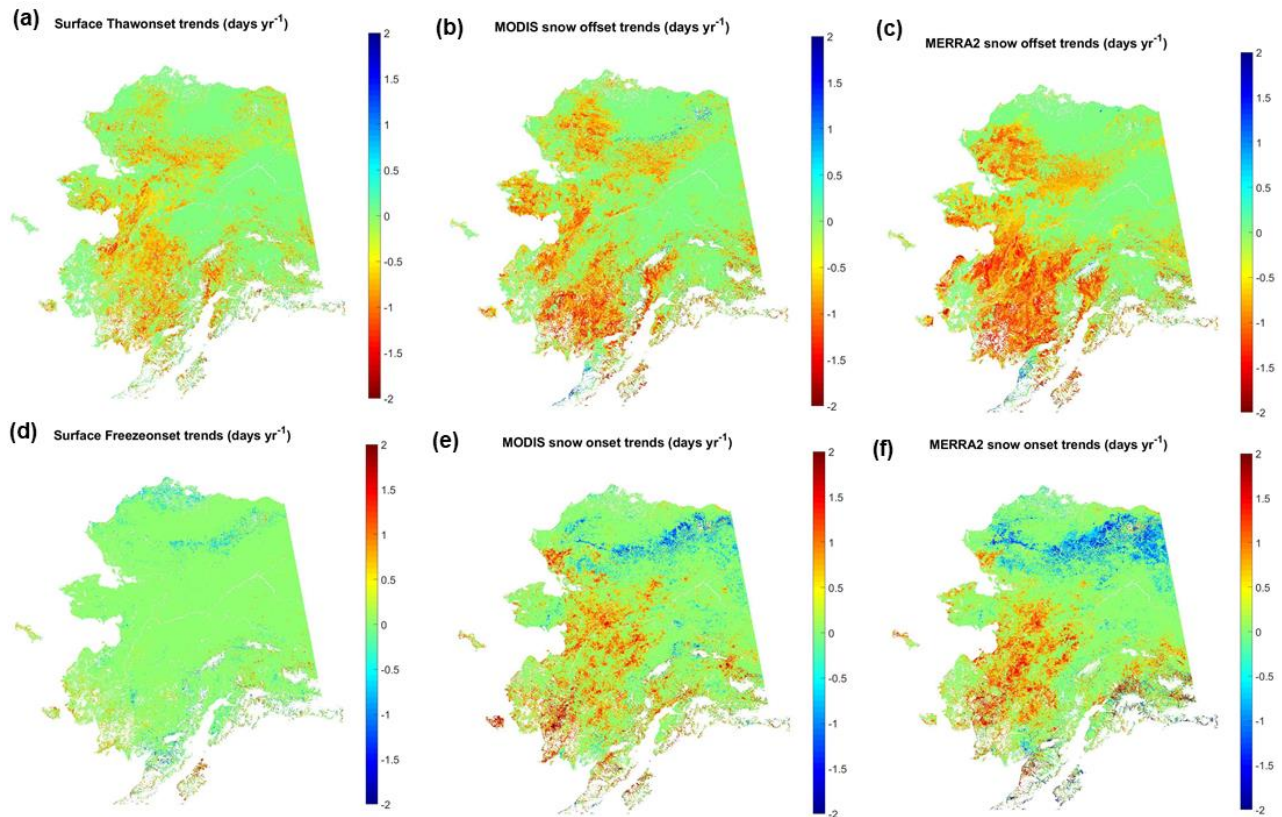
Fig. S8 Temporal (2001-2017) trends of surface freeze/thaw onset derived from MODIS LST data (a, d), snow offset/onset derived from MODIS SCE (b, e), and downscaled MERRA2 snow depth data (c, f). The timing of snow disappearance (i.e. snow offset) in the spring was defined as the center of the 8-day composite period being snow free, and with mean snow depth lower than 5 cm within a 24-day moving window.
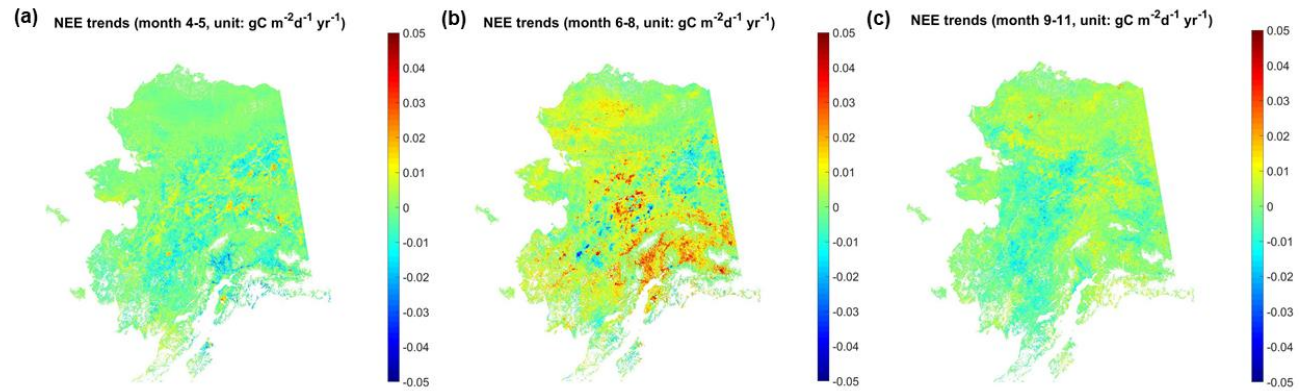
Fig. S9 Temporal (2001-2017) trends of model simulated seasonal NEE flux: (a) from April to May, (b) from June to August; (c) from September to November. Positive NEE trends indicate decreasing net carbon uptake activity, while negative NEE trends indicate enhanced net carbon uptake.